Electronic Supplementary Material (ESI) for Sustainable Energy & Fuels.

Supporting Information

P−Doped $CoCO_3$ Nanosheets: An Ultra−active Versatile Electrocatalyst for Hydrogen Evolution, Oxygen Evolution and Hydrazine Oxidation Reactions

*Fenggang Liu,[a] Huizhen Li,[*a] Yunhui Li,[a] Qinghe Cao[*c], Xinhua Geng,[a] Caiqin Gu,[a] Wenming Sun[*b] and Jiahai Wang[*a]*

[a]Guangzhou Key Laboratory for New Energy and Green Catalysis, School of Chemistry and Chemical Engineering, Guangzhou University, Guangzhou, 510006, P. R. China.

[b]College of Science, China Agricultural University, Beijing 100193, P. R. China.

[c]Frontiers Science Center for Flexible Electronics, Institute of Flexible Electronics, Northwestern Polytechnical University, Xi'an 710072, P. R. China.

Table of Contents

1. EXPERIMENTAL SECTION

Materials

$CO(NH_2)_2$, NH_4F, KOH, NaH_2PO_2, hydrazine, ethanol, hydrochloric acid, and acetone (Sinopharm Chemical Reagent Co., Ltd); Pt/C (20 wt% Pt, Shanghai Macklin Biochemical Co., Ltd); RuO_2 (Aladdin Ltd); Co Foam (KunShan Kunag Xun electronics Co., Ltd) were used as received.

Synthesis of $CoCO_3$ nanosheets on Co Foam

A piece of Co foam (1 cm × 4 cm) was sequentially cleaned by sonication in hydrochloric acid, ethanol and deionized water for 15 min, repectively. First, NH_4F (0.147 g, 5 mmol) and $CO(NH_2)_2$ (0.720 g, 12 mmol) were dissolved in deionized water (40 mL) with vigorous continuously stirring for 30 min, a clear solution was obtained. Second, the clear solution with a piece of dried Co foam were placed into a Teflon autoclave. In an electric oven, the autoclave was heated at 140 °C for 24 h to obtain $CoCO_3$ precursor.

Synthesis of P−$CoCO_3$ nanosheets on Co Foam

To prepare P−$CoCO_3$ samples, the $CoCO_3$ precursor was placed at the downstream side of a tube furnace and NaH_2PO_2 (3 g, 34 mmol) was placed at the opposite side. Then the samples were heated to 300 °C in Ar atmosphere for 90 min, and cooled down to room temperature naturally, and the P−$CoCO_3$ nanosheets was obtained.

Characterizations

X−ray diffraction (XRD) was carried out on a Bruker D8 ADVANCE

Diffractiometer (with Cu Kα radiation). X-ray photoelectron spectroscopy (XPS) measurements was measured on a Thermo Scientific Escalab 250Xi X-ray photoelectron spectrometer. SEM was implemented on a SU8010. TEM and HRTEM were conducted on a JEM-2100. EDS and EA were measured in a scanning (STEM) mode.

Electrochemical measurements

Electrochemical measurements were conducted on a CHI660E electrochemical workstation (CH Instruments, Inc., Shanghai). P−$CoCO_3$/CF was directly used as the working electrode, the graphite and saturated calomel electrode (SCE) were used as counter electrode and reference electrode, respectively. By using the Nernst equation E(RHE) = E(SCE) + 0.0591 pH + 0.2415 − 0.000761 (T − 298.15) (T: temperature), all of the data listed in this work were calibrated versus the RHE. LSV curves were obtained at a scan rate of 2 mV/s. The EIS were recorded at the frequency range of 100 -1 Hz with an AC amplitude of 5 mV.

Computational Details

By using the plane-wave pseudopotential method, DFT computations were carried out. The interaction of electron−ion was dealed with ultrasoft pseudopotentials, which created with the PBE functional.[1] For the electron wave functions, a plane−wave basis set was used and the kinetic energy cutoff is 380 eV.[1] The spin−unrestricted method was used in all calculations. For bulk $CoCO_3$, a 4×4×1 uniform *k*−point mesh was set as the Brillouin zone of the supercell. The optimized lattice constants for $CoCO_3$ are $a = b = 4.593$ Å, and $c = 15.063$ Å, which match well with them in database. [2] The (1×2)

$CoCO_3$ (104) slab with six atomic layers thickness (120 atoms included) was modeled to represent the $CoCO_3$ surface. The vacuum layer (15 Å) was used for avoiding the interactions among periodic images. Dipole moment correction was introduced. During optimization, only the top three layers were allowed to relax, where the total energy convergence is below 10^{-5} eV, and the maximum atomic forces is smaller than 0.03 eV/Å. Bu using the method of Norskov, the free energy diagrams of HzOR and HER were calculated according to the following equation $\Delta G = \Delta E + \Delta E_{ZPE} - T\Delta S$ (ΔE*:* the calculated total energy change; ΔE_{ZPE}: the calculated change in zero-point energy; ΔS: the calculated change in entropy). [3]

REFERENCES

(1) Perdew, J. P.; Burke, K.; Ernzerhof, M. Generalized Gradient Approximation Made Simple. *Phys. Rev. Lett.* **1996**, *77*, 3865–3868.

(2) Jain, A.; Ong, S. P.; Hautier, G.; Chen, W.; Richards, W. D.; Dacek, S.; Cholia, S.; Gunter, D.; Skinner, D.; Ceder, G.; Persson, K. A. Commentary: The Materials Project: A materials genome approach to accelerating materials innovation. *APL Materials* **2013**, *1*, 011002.

(3) Skúlason, E.; Tripkovic, V.; Björketun, M. E.; Gudmundsdóttir, S.; Karlberg, G.; Rossmeisl, J.; Bligaard, T.; Jónsson, H. Nørskov, J. K. Modeling the electrochemical hydrogen oxidation and evolution reactions on the basis of density functional theory calculations. *J. Phys. Chem. C* **2010**, *114*, 18182–18197.

2. SUPPORTING RESULTS

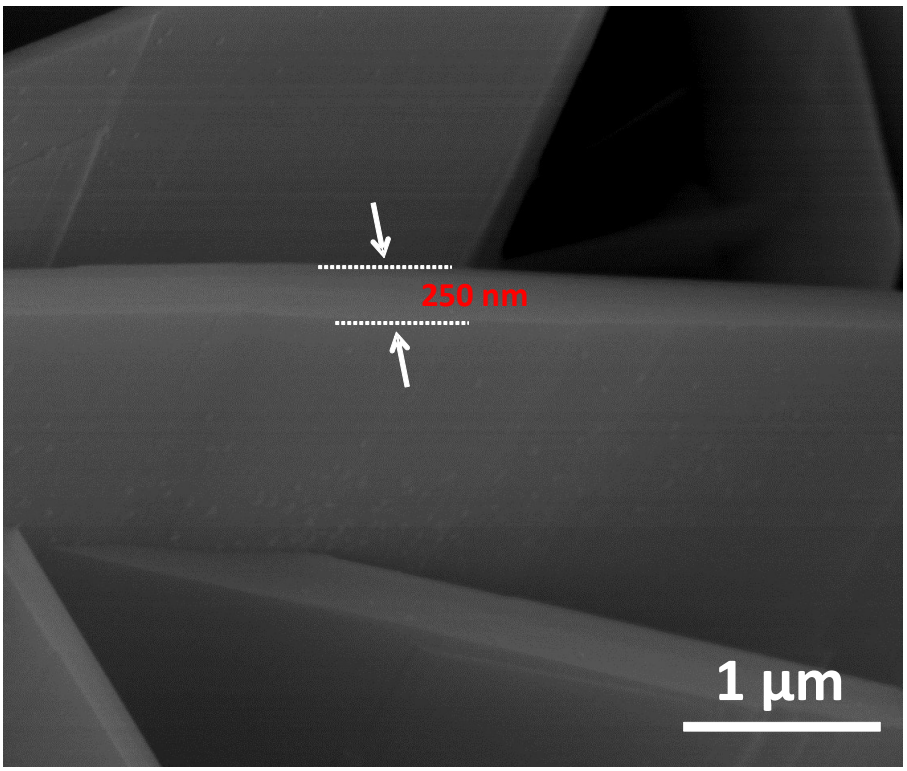

Fig. S1 SEM image of $CoCO_3$/CF.

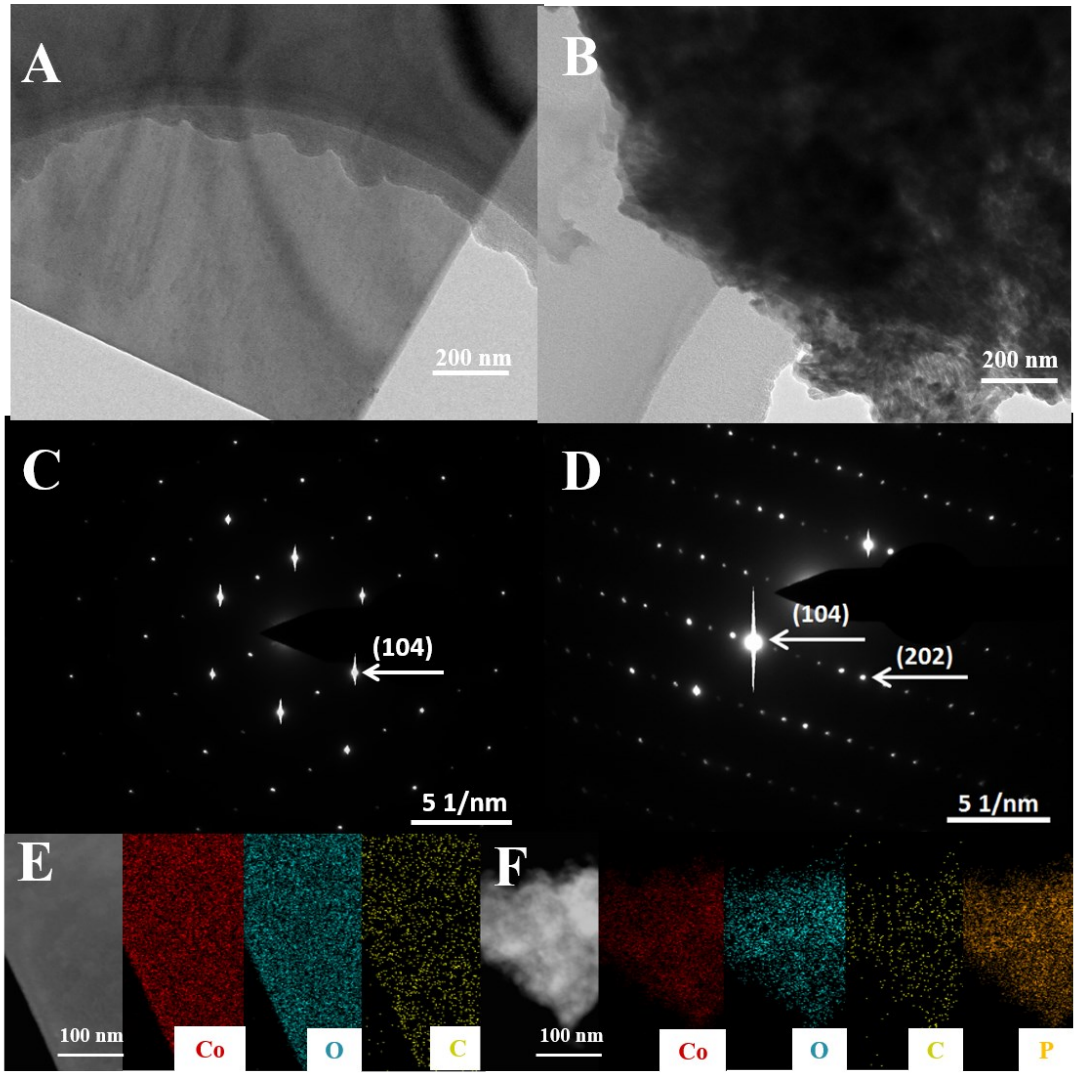

Fig. S2 A, B) Low-resolution TEM images; C, D) SAED patterns and E, F) Elemental mapping images of $CoCO_3$ and P-$CoCO_3$.

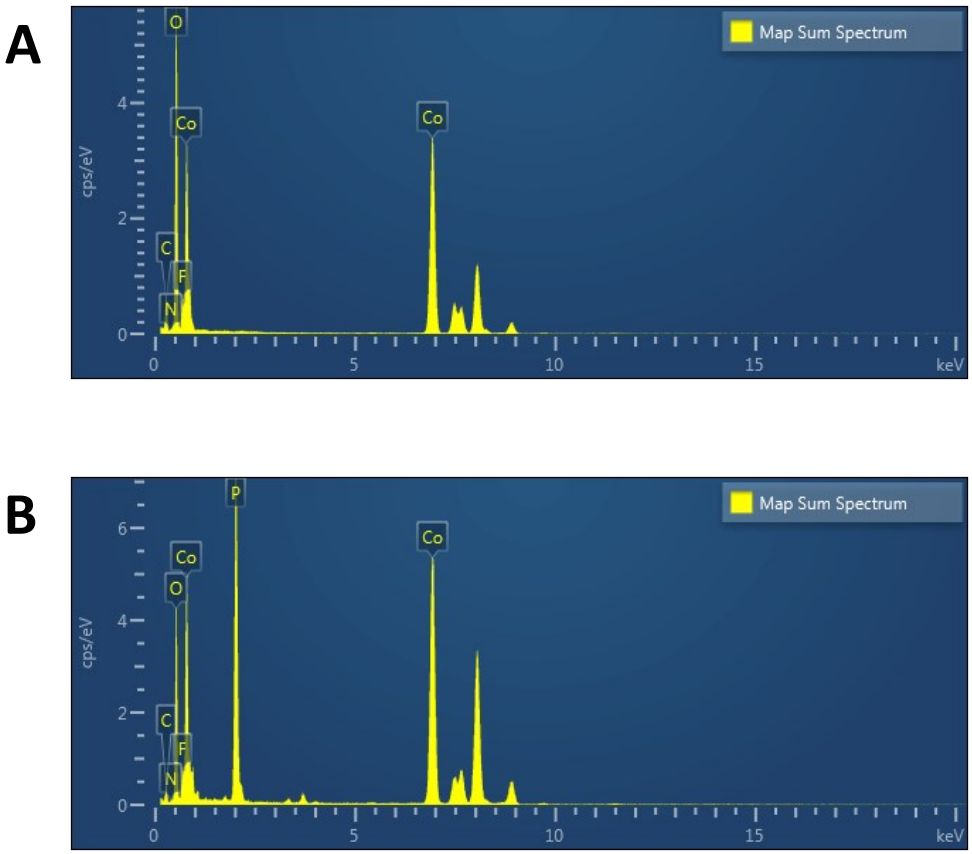

Fig. S3 TEM−EDS spectra of A) $CoCO_3$/CF and B) P−$CoCO_3$/CF.

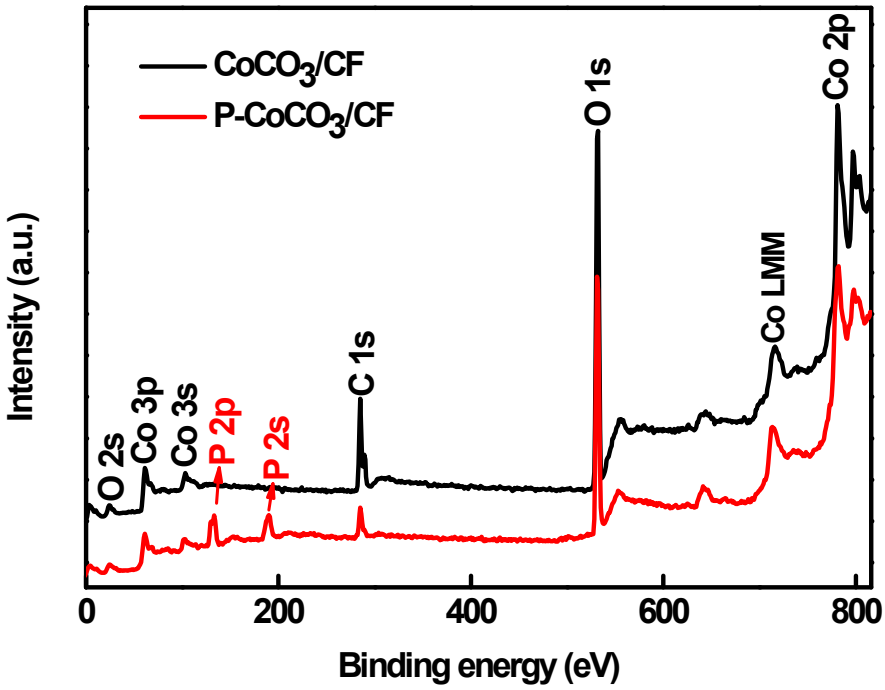

Fig. S4 Full XPS spectra of $CoCO_3$/CF and P−$CoCO_3$/CF.

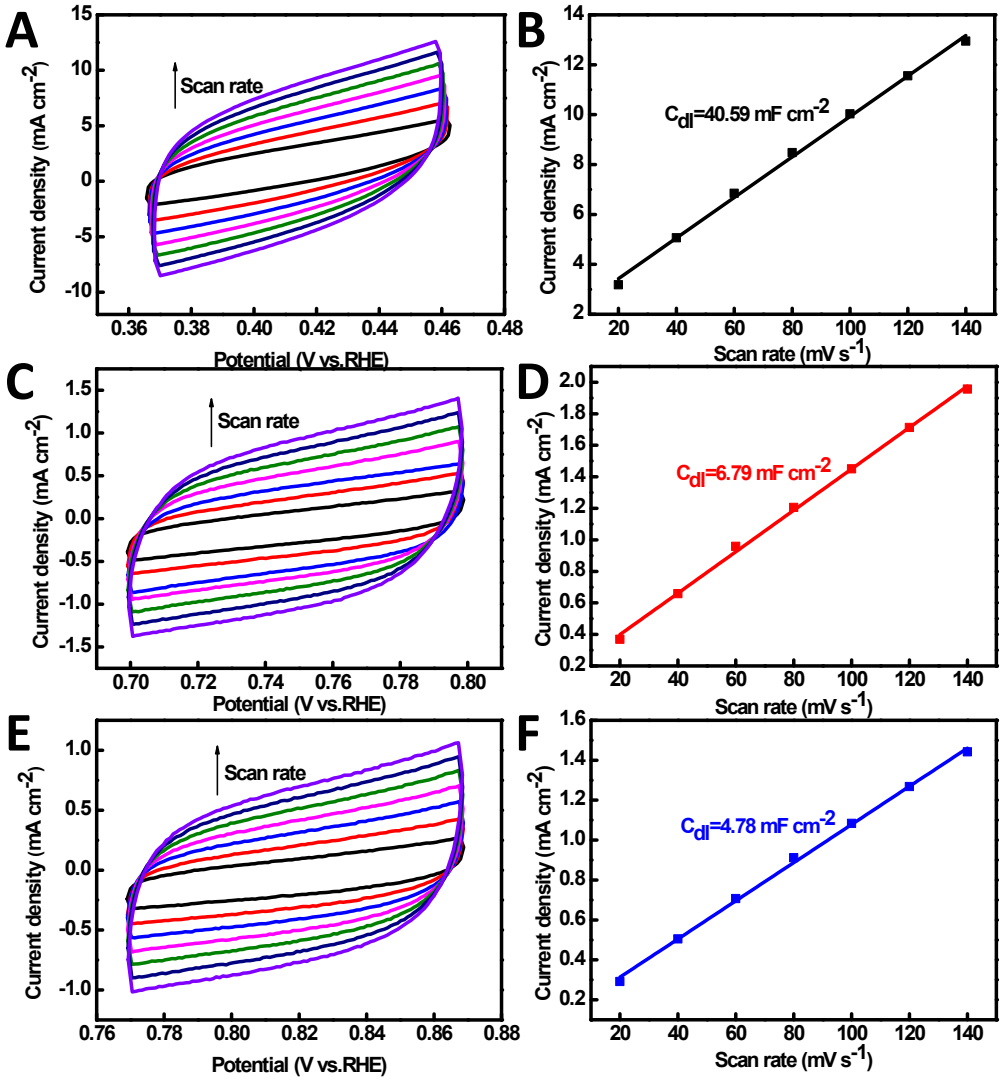

Fig. S5 CV curves of A) P−$CoCO_3$/CF, C) $CoCO_3$/CF and E) Co Foam at different scan rate in 1 M KOH in the non-faradaic potential region. Plots of current density versus voltage scan rate for B) P−$CoCO_3$/CF, D) $CoCO_3$/CF and F) Co Foam.

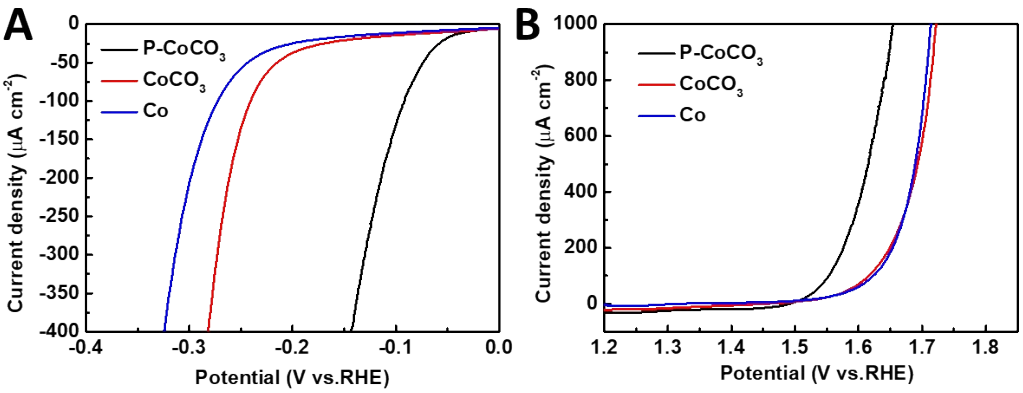

Fig. S6. LSV plots of P−$CoCO_3$, $CoCO_3$ and Co foam for A) HER and B) OER. The current densities are calculated based on ECSA.

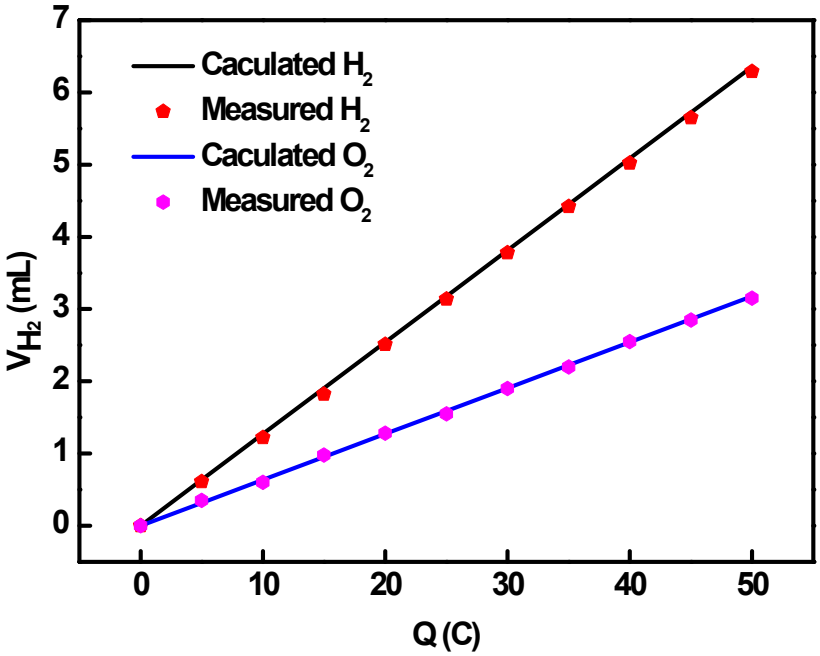

Fig. S7 Quantitative H_2 and O_2 measurement via water displacement.

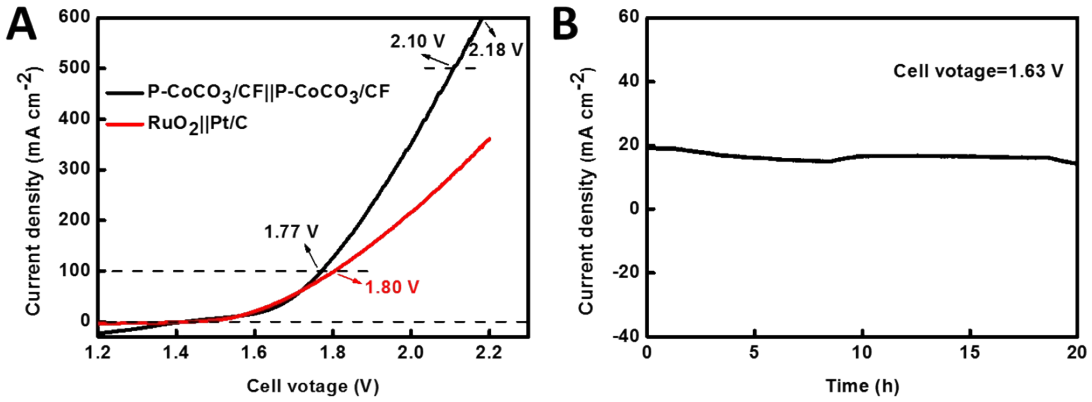

Fig. S8 Performance test for overall water splitting conducted in 1 M KOH. A) LSV curves of the P-$CoCO_3$(+)||P-$CoCO_3$(-) and RuO_2(+)||Pt/C(-) electrolytic system toward water splitting. B) Chronoamperometry of water electrolysis of the P-$CoCO_3$(+)||P-$CoCO_3$(-) system at a voltage of 1.63 V versus RHE.

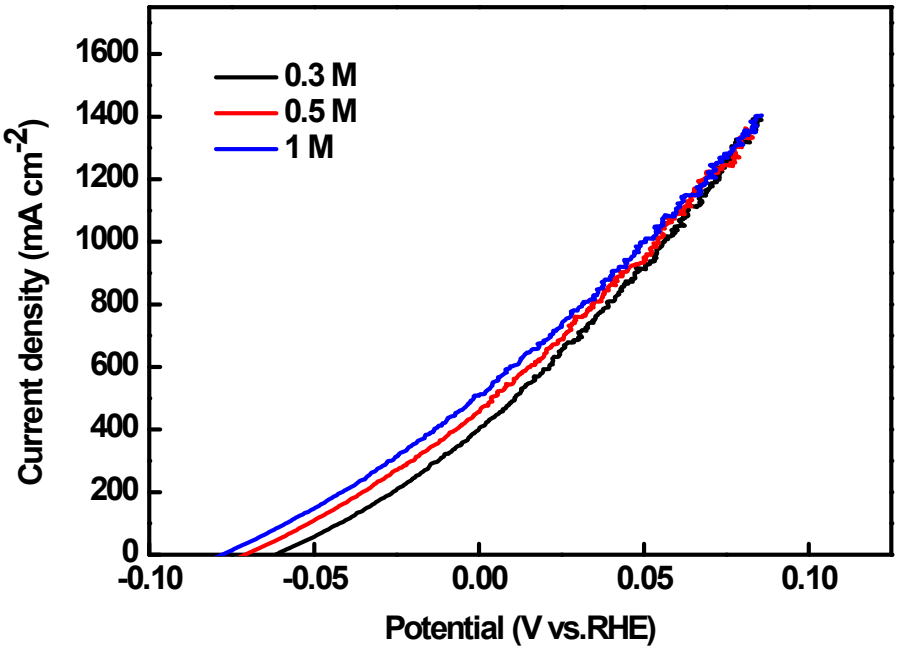

Fig. S9 LSV plots of P−$CoCO_3$/CF toward different concentrations of hydrazine (0.3~1 M).

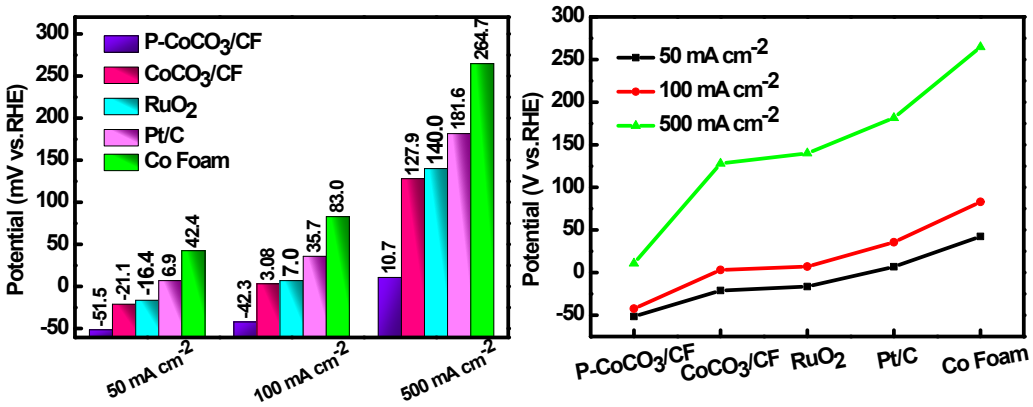

Fig. S10 The overpotentials needed of P−$CoCO_3$/CF, $CoCO_3$/CF, Co Foam, Pt/C and RuO_2 for HzOR (j = 50/100/500 mA cm^{-2}).

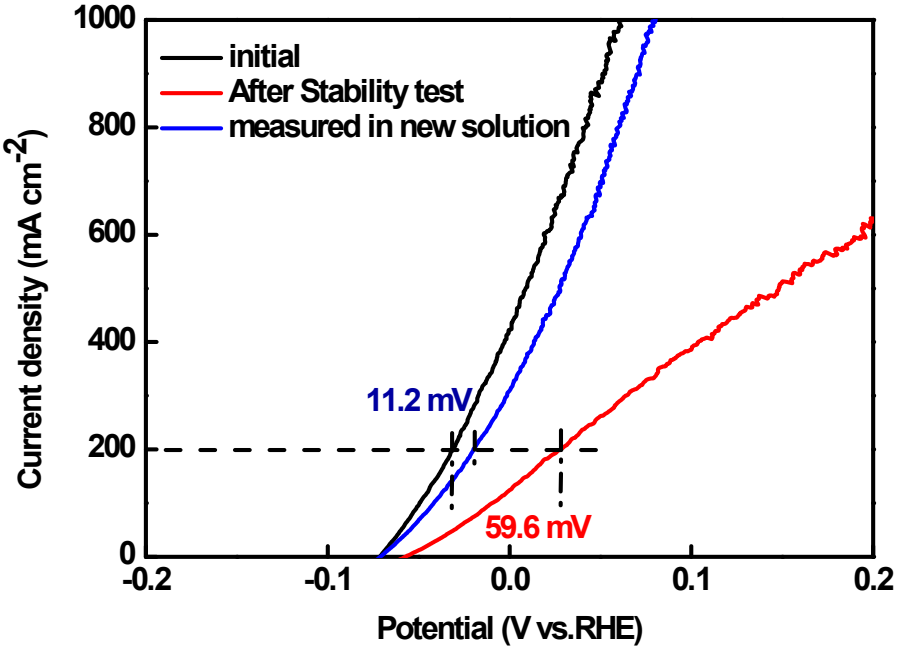

Fig. S11 LSV curves of P−$CoCO_3$/CF for initial and after stability test in 1 M KOH with 0.3 M hydrazine solution. Initial performance of P−$CoCO_3$/CF for HzOR (black line). The performance of P−$CoCO_3$/CF after stability test (red line). The performance of P−$CoCO_3$/CF after the stability test tested in the newly configured solution (blue line).

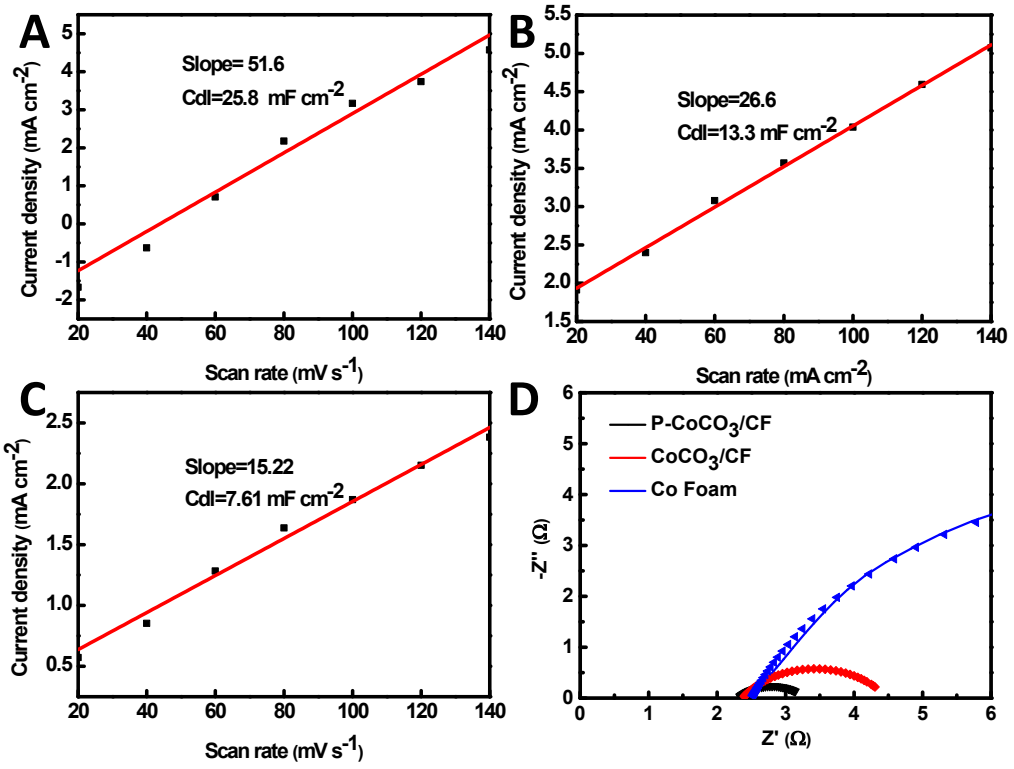

Fig. S12 A, B, C) Plots of current density versus voltage scan rate for P−$CoCO_3$/CF, $CoCO_3$/CF, Co Foam. D) Niquist plots together with their fits (scatter plot) for P−$CoCO_3$/CF, $CoCO_3$/CF, Co Foam. All of the experiments were carried out in 1.0 M KOH with 0.3 M hydrazine.

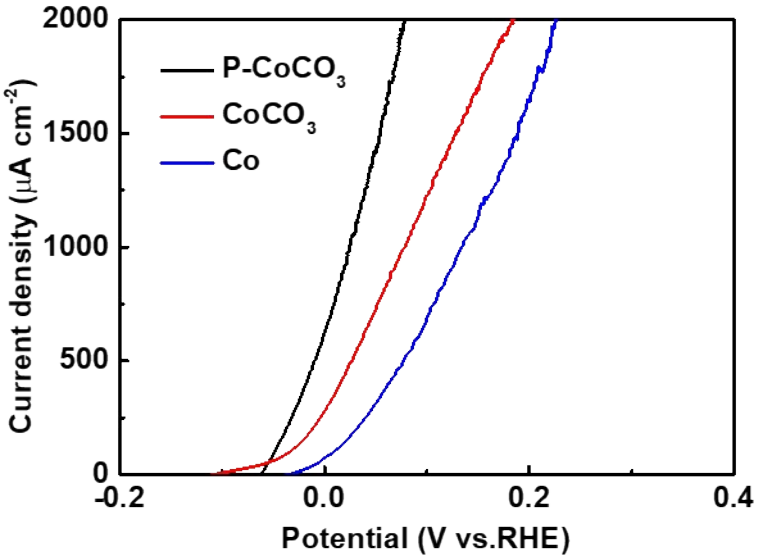

Fig. S13. LSV plots of P−$CoCO_3$, $CoCO_3$ and Co foam for HzOR. The current densities are calculated based on ECSA.

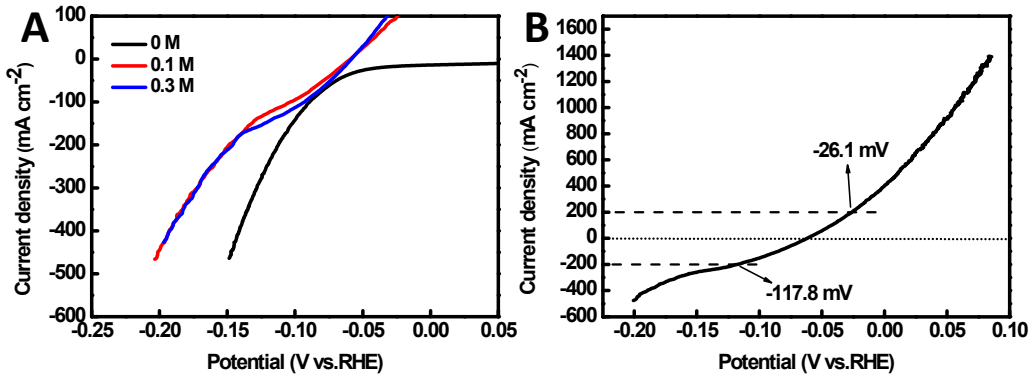

Fig. S14 A) LSV curves for the P−$CoCO_3$/CF toward different concentrations of hydrazine. B) LSV curves of P-$CoCO_3$/CF for the HER and HzOR in 1 M KOH with 0.3 M N_2H_4 solution.

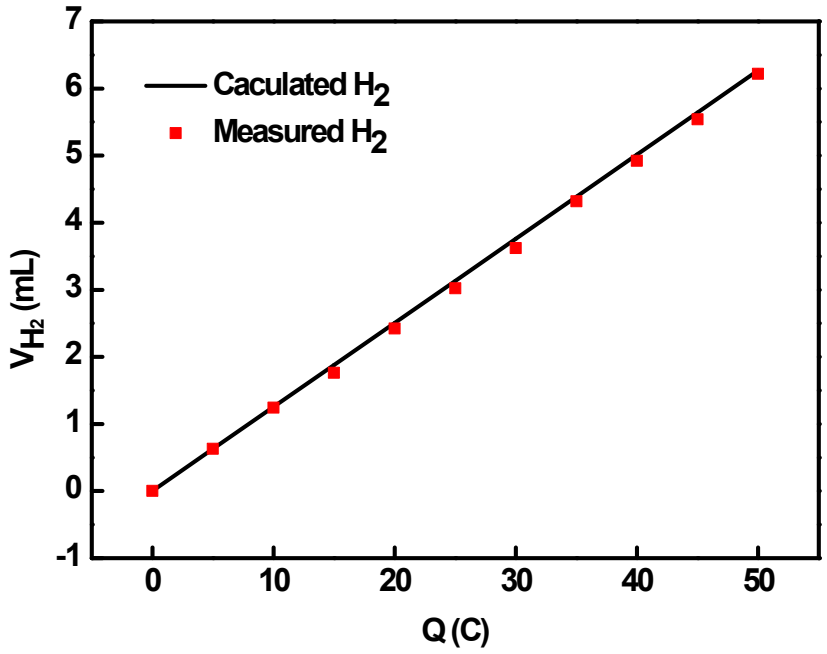

Fig. S15 Faraday efficiency measured for hydrogen production in 1 M KOH with 0.3 M N_2H_4 solution.

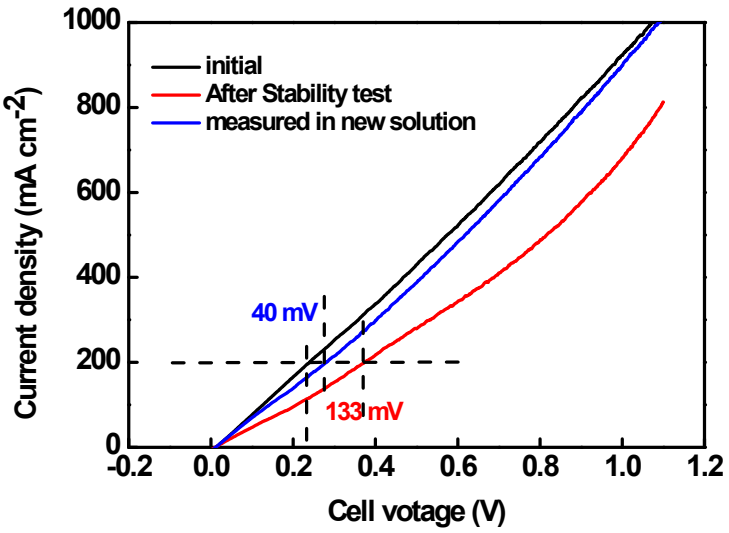

Fig. S16 LSV curves for the P−$CoCO_3$/CF(+)||P−$CoCO_3$/CF(−) couple for initial and after stability test in 1 M KOH with 0.3 M hydrazine solution. Initial performance of P−$CoCO_3$/CF(+)||P−$CoCO_3$/CF(−) couple for HzOR (black line). The performance of P−$CoCO_3$/CF(+)||P−$CoCO_3$/CF(−) couple after stability test (red line). The performance of P−$CoCO_3$/CF(+)||P−$CoCO_3$/CF(−) couple after the stability test tested in the newly configured solution (blue line).

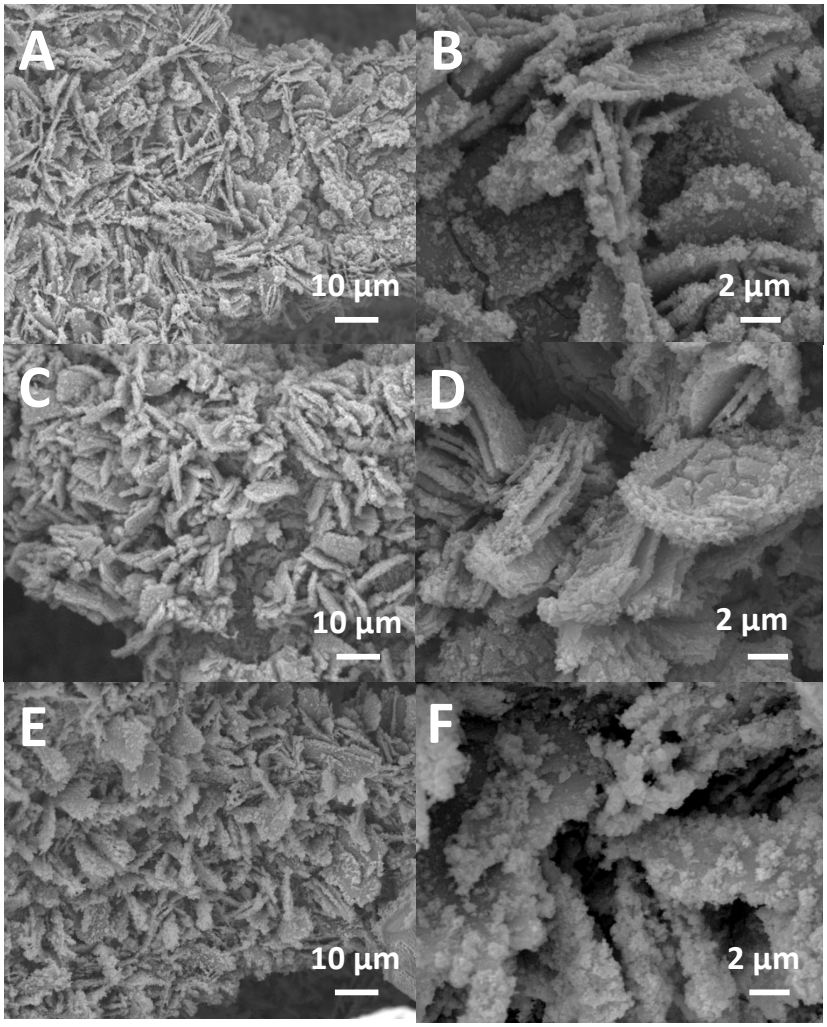

Fig. S17 SEM images of P−$CoCO_3$/CF after A, B) HER, C, D) OER and E, F) HzOR stability test.

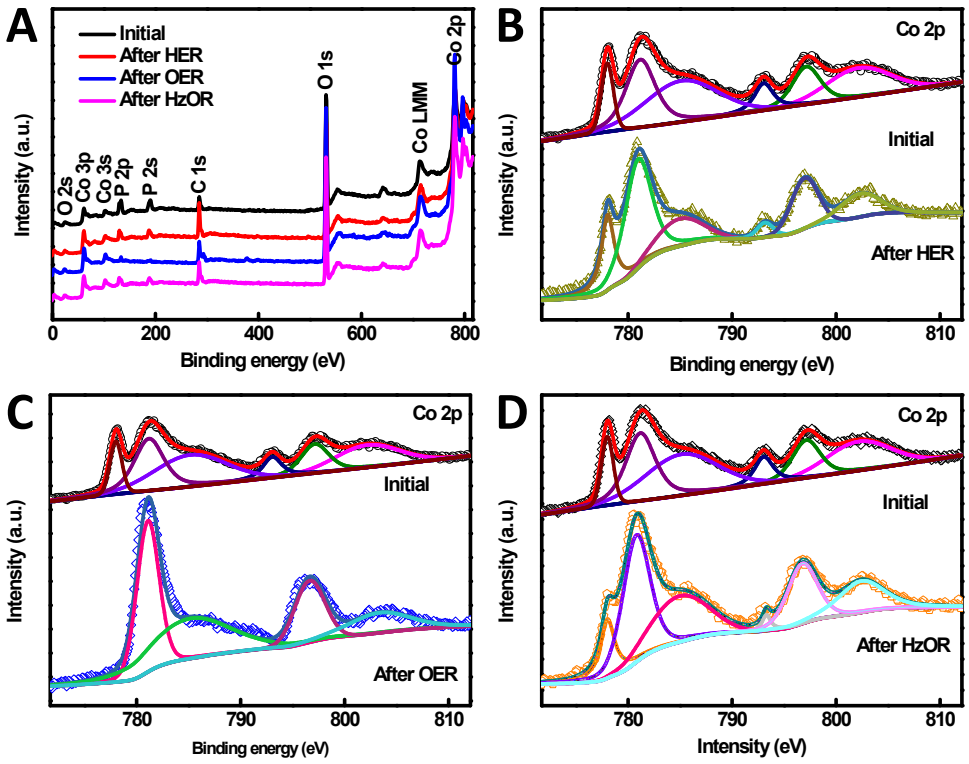

Fig. S18 A) XPS full spectrum of P−$CoCO_3$/CF before and after the anode and cathode catalysis. B) XPS spectra of Co 2p for P−$CoCO_3$/CF before and after HER test. C) XPS spectra of Co 2p for P−$CoCO_3$/CF before and after OER test. D) XPS spectra of Co 2p for P−$CoCO_3$/CF before and after HzOR test.

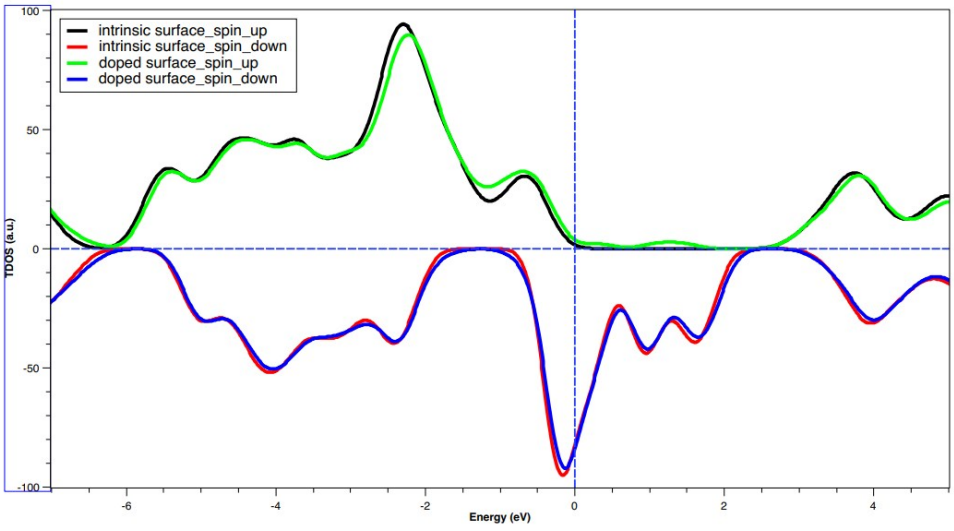

Fig. S19. Total DOS of $CoCO_3$ and P−$CoCO_3$ (104) surface. The positive and negative values of PDOS indicated the up and down spins, respectively.

Table S1 The elements content in P-$CoCO_3$/CF derived from XPS.

Element	Co	C	O	P
Rate (%)	14.6	15.6	51.1	18.7

Table S2 Comparisons of HER performances of P−$CoCO_3$/CF with other cost-effective metal HER catalysts in 1.0 M KOH.

Catalyst	**j (mA cm^{-2})**	**Potential (V)**	**Refs.**
Co/CoP	10	253	S1
NESSP	10	230	S2
O-Co_2P	10	160	S3
Ni_3FeN/rGO	10	158	S4
EG/H-$Co_{0.85}Se$|P	10	150	S5
$Co_{0.9}S_{0.58}P_{0.42}$	10	141	S6
Cu@CoS_x/NF	10	134	S7
P-Co_3O_4	10	120	S8
CoP/NCNHP	10	115	S9
$P_{8.6}$-Co_3O_4/NF	10	97	S10
Fe-CoP/Ti	10	78	S11
Fe-Ni_3C	10	178	S12
VOOH	10	164	S13
$CoSe_2$	10	79	S14
Ni-Co-P	10	107	S15
Cu@NiFe LDH	10	116	S16
FeS_2	10	96	S17
Co_1Mn_1CH	10	180	S18
O3-V10-Ni_2P	10	147	S19
$Ni_{1.5}Fe_{0.5}P$	10	282	S20
CoMoP@C	10	81	S21
P-$CoCO_3$/CF	10	46	This work

Table S3 Comparisons of OER performances of P−$CoCO_3$/CF with other cost-effective metal OER catalysts in 1.0 M KOH.

Catalyst	**j (mA cm^{-2})**	**Potential (V)**	**Refs.**
Co/CoP	10	340	S1
Ni_3FeN/rGO	10	280	S4
P-Co_3O_4	10	280	S8
CoP/NCNHP	10	310	S9
ACP	10	364	S22
Co_9S_8	10	340	S23
CoPS@NPS-C	10	320	S24
Co(OH)F	10	313	S25
Mo-CoOOH	10	305	S26
S:CoP/NF	10	300	S27
NiFeOF	10	295	S28
B,N:Mo_2C@BCN	10	290	S29
NiCo@$NiCoO_2$/C	20	366	S30
Co-Ni_3N	10	307	S31
$NiSe_2$	10	330	S32
P-$CoCO_3$/CF	10/20	275/285	This work

Table S4 Comparisons of overall water-splitting performance of P−$CoCO_3$/CF||P−$CoCO_3$/CF with other cost-effective metal bifunctional catalysts in 1.0 M KOH.

Catalyst	**j (mA cm^{-2})**	**Potential (V)**	**Refs.**
NESSP||NESSP	10	510	S2
Ni_3FeN/rGO||Ni_3FeN/rGO	10	370	S4
EG/H-$Co_{0.85}Se$|P||EG/H-$Co_{0.85}Se$|P	10	410	S5
$Co_{0.9}Se_{0.58}P_{0.42}$||$Co_{0.9}Se_{0.58}P_{0.42}$	10	360	S6
Cu@CoS_x/NF||Cu@CoS_x/NF	100	570	S7
P-Co_3O_4||P-Co_3O_4	50	530	S8
CoP/NCNHP||CoP/NCNHP	10	410	S9
$P_{8.6}$-Co_3O_4/NF||$P_{8.6}$-Co_3O_4/NF	10	400	S10
Fe-CoP/Ti ||Fe-CoP/Ti	10	370	S11
VOOH ||VOOH	10	390	S13
Ni-Co-P||Ni-Co-P	10	390	S15
Co_1Mn_1CH||Co_1Mn_1CH	10	450	S18
O3-V10-Ni_2P||O3-V10-Ni_2P	10	333	S19
$Ni_{1.5}Fe_{0.5}P$||$Ni_{1.5}Fe_{0.5}P$	10	359	S20
Co_9S_8||Co_9S_8	10	370	S23
CoPS@NPS-C||CoPS@NPS-C	10	390	S24
Mo-CoP||Mo-CoOOH	10	330	S26
S:CoP/NF||S:CoP/NF	100	550	S27
NiFeOF||NiFeOF	10	600	S28
Co_3O_4-MTA||Co_3O_4-MTA	10	400	S33
Ni_2Fe_1-O|| Ni_2Fe_1-O	10	410	S34
FeB_2||FeB_2	10	340	S35
$Ni_{11}(HPO_3)_8(OH)_6$|| $Ni_{11}(HPO_3)_8(OH)_6$	10	370	S36
P-$CoCO_3$/CF|| P-$CoCO_3$/CF	10/50/100	319/471/541	This work

Table S5. Comparisons of HzOR performances of P−$CoCO_3$/CF with other HzOR catalysts.

Catalyst	**Electrolyte**	**j (mA cm^{-2})**	**Potential (V)**	**Refs.**
$CoSe_2$	1 M KOH + 0.5 M N_2H_4	100	170	S14
Ni-Zn alloys	1 M NaOH + 0.1 M N_2H_4	300	400	S37
CoNiS	0.1 M KOH + 2 M N_2H_4	147	1200	S38
Cu_3P/CF	1 M KOH + 0.5 M N_2H_4	50	98	S39
Ni_3S_2/NF	1 M KOH + 0.2 M N_2H_4	100	415	S40
$Ni_{0.5}Co_{0.5}Se_2$/CC	1 M KOH + 0.5 M N_2H_4	50	8	S41
Ni_3Se_4	1 M KOH + 0.1 M N_2H_4	10	370	S42
Ni(Cu)/NF	1 M KOH + 0.5 M N_2H_4	50	38	S43
$Pt_{0.2}Ni_{0.8}$	1 M KOH + 0.1 M N_2H_4	44	500	S44
Ni_2P/NF	1 M KOH + 0.5 M N_2H_4	50	-25	S45
CoP/TiM	1 M KOH + 0.1 M N_2H_4	100	-6	S46
FeP/NF	1 M KOH + 0.5 M N_2H_4	10	18	S47
CoS_2/TiM	1 M KOH + 0.1 M N_2H_4	150	170	S48
NiS_2/TiM	1 M KOH + 0.5 M N_2H_4	300	218	S49
3D-PNNF	1 M KOH + 1 M N_2H_4	250	198.6	S50
P-$CoCO_3$/CF	1 M KOH + 0.3 M N_2H_4	50/100/300	-51.5/-42.3/-12.3	This work

Table S6. Lists of applied voltage for H_2 production from water electrolysis assisted by small molecules oxidation in recent reports.

Catalyst	**Electrolyte**	**j (mA cm^{-2})**	**Potential (V)**	**Refs.**
$CoSe_2$||$CoSe_2$	1 M KOH + 0.5 M N_2H_4	10	0.165	S14
Cu_3P/CF||Cu_3P/CF	1 M KOH + 0.5 M N_2H_4	100	0.72	S39
Ni_3S_2/NF||Ni_3S_2/NF	1 M KOH + 0.2 M N_2H_4	100	0.867	S40
$Ni_{0.5}Co_{0.5}Se_2$/CC||$Ni_{0.5}Co_{0.5}Se_2$/CC	1 M KOH + 0.5 M N_2H_4	10	0.14	S41
Ni(Cu)/NF||Ni(Cu)/NF	1 M KOH + 0.5 M N_2H_4	100	0.41	S43
Ni_2P/NF|| Ni_2P/NF	1 M KOH + 0.5 M N_2H_4	100	0.45	S45
CoP/TiM||CoP/TiM	1 M KOH + 0.1 M N_2H_4	10	0.2	S46
FeP/NF|| FeP/NF	1 M KOH + 0.5 M N_2H_4	125	0.5	S47
CoS_2/TiM ||CoS_2/TiM	1 M KOH + 0.1 M N_2H_4	100	0.81	S48
NiS_2/TiM ||NiS_2/TiM	1 M KOH + 0.5 M N_2H_4	10	0.34	S49
S-MnO_2||S-MnO_2	1 M KOH + 0.5 M urea	10	1.41	S51
$Zn_{0.08}Co_{0.92}P$/TM ||$Zn_{0.08}Co_{0.92}P$/TM	1 M KOH + 0.5 M urea	10	1.38	S52
NiCoP/CC||NiCoP/CC	1 M KOH + 0.33 M urea	20	1.25	S53
Ni_3N/CC||Ni_3N/CC	1 M KOH + 0.33 M urea	10	1.44	S54
Ni_2P/CC||Ni_2P/CC	1 M KOH + 0.5 M urea	50	1.35	S55
Fe-CoP/CC||Fe-CoP/CC	1 M KOH + 5 mL AE	10	1.44	S56
Ni_2P NPA/NF||Ni_2P NPA/NF	1 M KOH + 10 mM HMF	10	1.65	S57
hp-Ni||hp-Ni	1 M KOH + 10 mM EtOH	10	1.50	S58
P-$CoCO_3$/CF|| P-$CoCO_3$/CF	1 M KOH + 0.3 M N_2H_4	100	0.13	This work

Table S7. Bond lengths of all the species (Å).

	Co-N	N-N		Co-N	N-N	Clean-surface	delta Co-N	delta N-N
free N_2H_4	1.961	1.438	free N_2H_4		1.438			
N_2H_4	1.896	1.436	N_2H_4	1.994	1.435	N_2H_4	-0.033	0.001
N_2H_3	1.825	1.360	N_2H_3	1.942	1.371	N_2H_3	-0.046	-0.011
N_2H_2	1.836	1.276	N_2H_2	1.841	1.279	N_2H_2	-0.016	-0.003
N_2H_1	1.817	1.247	N_2H_1	1.826	1.253	N_2H_1	0.010	-0.006
N_2H_0		1.167	N_2H_0	1.818	1.168	N_2H_0	-0.001	-0.001
free N_2		1.159	free N_2		1.159			

REFERENCE

S1. Xue, Z.-H.; Su, H.; Yu, Q.-Y.; Zhang, B.; Wang, H.-H.; Li, X.-H.; Chen, J.-S., Janus Co/CoP Nanoparticles as Efficient Mott-Schottky Electrocatalysts for Overall Water Splitting in Wide pH Range. Adv. Energy Mater. 2017, 7, 1602355.

S2. Balogun, M.-S.; Qiu, W.; Huang, Y.; Yang, H.; Xu, R.; Zhao, W.; Li, G.-R.; Ji, H.; Tong, Y., Cost-Effective Alkaline Water Electrolysis Based on Nitrogen- and Phosphorus-Doped Self-Supportive Electrocatalysts. Adv. Mater. 2017, 29, 1702095.

S3. Xu, K.; Ding, H.; Zhang, M.; Chen, M.; Hao, Z.; Zhang, L.; Wu, C.; Xie, Y., Regulating Water-Reduction Kinetics in Cobalt Phosphide for Enhancing HER Catalytic Activity in Alkaline Solution. Adv. Mater. 2017, 29, 1606980.

S4. Gu, Y.; Chen, S.; Ren, J.; Jia, Y. A.; Chen, C.; Komarneni, S.; Yang, D.; Yao, X., Electronic Structure Tuning in Ni_3FeN/r-GO Aerogel toward Bifunctional Electrocatalyst for Overall Water Splitting. ACS Nano 2018, 12 (1), 245-253.

S5. Hou, Y.; Qiu, M.; Zhang, T.; Zhuang, X.; Kim, C.-S.; Yuan, C.; Feng, X., Ternary Porous Cobalt Phosphoselenide Nanosheets: An Efficient Electrocatalyst for Electrocatalytic and Photoelectrochemical Water Splitting. Adv. Mater. 2017, 29, 1701589.

S6. Dai, Z.; Geng, H.; Wang, J.; Luo, Y.; Li, B.; Zong, Y.; Yang, J.; Guo, Y.; Zheng, Y.; Wang, X.; Yan, Q., Hexagonal-Phase Cobalt Monophosphosulfide for Highly Efficient Overall Water Splitting. ACS Nano 2017, 11 (11), 11031-11040.

S7. Liu, Y.; Li, Q.; Si, R.; Li, G.-D.; Li, W.; Liu, D.-P.; Wang, D.; Sun, L.; Zhang, Y.; Zou, X., Coupling Sub-Nanometric Copper Clusters with Quasi-Amorphous Cobalt Sulfide Yields Efficient and Robust Electrocatalysts for Water Splitting Reaction. Adv. Mater. 2017, 29, 1606200.

S8. Xiao, Z.; Wang, Y.; Huang, Y.-C.; Wei, Z.; Dong, C.-L.; Ma, J.; Shen, S.; Li, Y.; Wang, S., Filling the Oxygen Vacancies in Co_3O_4 with Phosphorus: an Ultra-efficient Electrocatalyst for overall water splitting. Energy Environ. Sci., 2017, 10, 2563-2569.

S9. Pan, Y.; Sun, K.; Liu, S.; Cao, X.; Wu, K.; Cheong, W.-C.; Chen, Z.; Wang, Y.; Li, Y.; Liu, Y.; Wang, D.; Peng, Q.; Chen, C.; Li, Y., Core-Shell ZIF-8@ZIF-67-

Derived CoP Nanoparticle-Embedded N-Doped Carbon Nanotube Hollow Polyhedron for Efficient Overall Water Splitting. *J. Am. Chem. Soc.* 2018, 140, 2610-2618.

S10. Wang, Z.; Liu, H.; Ge, R.; Ren, X.; Ren, J.; Yang, D.; Zhang, L.; Sun, X., Phosphorus-Doped Co_3O_4 Nanowire Array: A Highly Efficient Bifunctional Electrocatalyst for Overall Water Splitting. ACS Catal. 2018, 8, 2236-2241.

S11. Tang, C.; Zhang, R.; Lu, W.; He, L.; Jiang, X.; Asiri, A. M.; Sun, X., Fe-Doped CoP Nanoarray: A Monolithic Multifunctional Catalyst for Highly Efficient Hydrogen Generation. Adv. Mater. 2017, 29, 1602441.

S12. Fan, H.; Yu, H.; Zhang, Y.; Zheng, Y.; Luo, Y.; Dai, Z.; Li, B.; Zong, Y.; Yan, Q., Fe-Doped Ni_3C Nanodots in N-Doped Carbon Nanosheets for Efficient Hydrogen-Evolution and Oxygen-Evolution Electrocatalysis. Angew. Chem. Int. Ed. 2017, 56, 12566-12570.

S13. Shi, H.; Liang, H.; Ming, F.; Wang, Z., Efficient Overall Water-Splitting Electrocatalysis Using Lepidocrocite VOOH Hollow Nanospheres. Angew. Chem. Int. Ed. 2017, 56, 573-577.

S14. Zhang, J.-Y.; Wang, H.; Tian, Y.; Yan, Y.; Xue, Q.; He, T.; Liu, H.; Wang, C.; Chen, Y.; Xia, B. Y., Anodic Hydrazine Oxidation Assists Energy-Efficient Hydrogen Evolution over a Bifunctional Cobalt Perselenide Nanosheet Electrode. Angew. Chem. Int. Ed. 2018, 57, 7649-7653.

S15. Hu, E.; Feng, Y.; Nai, J.; Zhao, D.; Hu, Y.; Lou, X. W., Construction of Hierarchical Ni-Co-P Hollow Nanobricks with Oriented Nanosheets for Efficient Overall Water Splitting. Energy Environ. Sci., 2018, 11, 872-880.

S16. Yu, L.; Zhou, H.; Sun, J.; Qin, F.; Yu, F.; Bao, J.; Yu, Y.; Chen, S.; Ren, Z., Cu Nanowires Shelled with NiFe Layered Double Hydroxide Nanosheets as Bifunctional Electrocatalysts for Overall Water Splitting. Energy Environ. Sci., 2017, 10, 1820-1827.

S17. Miao, R.; Dutta, B.; Sahoo, S.; He, J.; Zhong, W.; Cetegen, S. A.; Jiang, T.; Alpay, S. P.; Suib, S. L., Mesoporous Iron Sulfide for Highly Efficient Electrocatalytic Hydrogen Evolution. J. Am. Chem. Soc. 2017, 139, 13604-13607.

S18. Tang, T.; Jiang, W. J.; Niu, S.; Liu, N.; Luo, H.; Chen, Y.-Y.; Jin, S.-F.; Gao, F.;

Wan, L.-J.; Hu, J.-S., Electronic and Morphological Dual Modulation of Cobalt Carbonate Hydroxides by Mn Doping toward Highly Efficient and Stable Bifunctional Electrocatalysts for Overall Water Splitting. *J. Am. Chem. Soc.* 2017, 139, 8320-8328.

S19. Dinh, K. N.; Sun, X.; Dai, Z.; Zheng, Y.; Zheng, P.; Yang, J.; Xu, J.; Wang, Z.; Yan, Q., O_2 Plasma and Cation Tuned Nickel Phosphide Nanosheets for Highly Efficient Overall Water Splitting. Nano Energy 2018, 54, 82-90.

S20. Huang, H.; Yu, C.; Zhao, C.; Han, X.; Yang, J.; Liu, Z.; Li, S.; Zhang, M.; Qiu, J., Iron-tuned Super Nickel Phosphide Microstructures with High Activity for Electrochemical Overall Water Splitting. Nano Energy 2017, 34, 472-480.

S21. Ma, Y.-Y.; Wu, C.-X.; Feng, X.-J.; Tan, H.-Q.; Yan, L.-K.; Liu, Y.; Kang, Z.-H.; Wang, E.-B.; Li, Y.-G., Highly Efficient Hydrogen Evolution from Seawater by a Low-cost and Stable CoMoP@C Electrocatalyst Superior to Pt/C. Energy Environ. Sci., 2017, 10, 788-798.

S22. Kim, J. S.; Park, I.; Jeong, E.-S.; Jin, K.; Seong, W. M.; Yoon, G.; Kim, H.; Kim, B.; Nam, K. T.; Kang, K., Amorphous Cobalt Phyllosilicate with Layered Crystalline Motifs as Water Oxidation Catalyst. Adv. Mater. 2017, 29, 1606893.

S23. Huang, S.; Meng, Y.; He, S.; Goswami, A.; Wu, Q.; Li, J.; Tong, S.; Asefa, T.; Wu, M., N-, O-, and S-Tridoped Carbon-Encapsulated Co_9S_8 Nanomaterials: Efficient Bifunctional Electrocatalysts for Overall Water Splitting. Adv. Funct. Mater. 2017, 27, 1606585.

S24. Hu, Y.; Li, F.; Long, Y.; Yang, H.; Gao, L.; Long, X.; Hu, H.; Xu, N.; Jin, J.; Ma, J., Ultrafine CoPS Nanoparticles Encapsulated in N, P, and S tri-doped Porous Carbon as an Efficient Bifunctional Water Splitting Electrocatalyst in Both Acid and Alkaline Solutions. J. Mater. Chem. A 2018, 6, 10433-10440.

S25. Wan, S.; Qi, J.; Zhang, W.; Wang, W.; Zhang, S.; Liu, K.; Zheng, H.; Sun, J.; Wang, S.; Cao, R., Hierarchical Co(OH)F Superstructure Built by Low-Dimensional Substructures for Electrocatalytic Water Oxidation. Adv. Mater. 2017, 29, 1700286.

S26. Guan, C.; Xiao, W.; Wu, H.; Liu, X.; Zang, W.; Zhang, H.; Ding, J.; Feng, Y. P.; Pennycook, S. J.; Wang, J., Hollow Mo-doped CoP nanoarrays for efficient overall water splitting. Nano Energy 2018, 48, 73-80.

S27. Anjum, M. A. R.; Okyay, M. S.; Kim, M.; Lee, M. H.; Park, N.; Lee, J. S., Bifunctional Sulfur-doped Cobalt Phosphide Electrocatalyst Outperforms All-noble-metal Electrocatalysts in Alkaline Electrolyzer for Overall Water Splitting. Nano Energy 2018, 53, 286-295.

S28. Liang, K.; Guo, L.; Marcus, K.; Zhang, S.; Yang, Z.; Perea, D. E.; Zhou, L.; Du, Y.; Yang, Y., Overall Water Splitting with Room-Temperature Synthesized NiFe Oxyfluoride Nanoporous Films. *ACS Catal.* 2017, 7, 8406-8412.

S29. Anjum, M. A. R.; Lee, M. H.; Lee, J. S., Boron and Nitrogen Co-doped Molybdenum Carbide Nanoparticles Imbedded in BCN Network as a Bifunctional Electrocatalyst for Hydrogen and Oxygen Evolution Reactions. *ACS Catal.* 2018, 8296-8305.

S30. Xu, H.; Shi, Z.-X.; Tong, Y.-X.; Li, G.-R., Porous Microrod Arrays Constructed by Carbon-Confined NiCo@$NiCoO_2$ Core@Shell Nanoparticles as Efficient Electrocatalysts for Oxygen Evolution. Adv. Mater. 2018, 30, 1705442.

S31. Zhu, C.; Wang, A.-L.; Xiao, W.; Chao, D.; Zhang, X.; Tiep, N. H.; Chen, S.; Kang, J.; Wang, X.; Ding, J.; Wang, J.; Zhang, H.; Fan, H. J., In Situ Grown Epitaxial Heterojunction Exhibits High-Performance Electrocatalytic Water Splitting. Adv Mater 2018, 30, 1705516.

S32. Chen, S.; Kang, Z.; Hu, X.; Zhang, X.; Wang, H.; Xie, J.; Zheng, X.; Yan, W.; Pan, B.; Xie, Y., Delocalized Spin States in 2D Atomic Layers Realizing Enhanced Electrocatalytic Oxygen Evolution. Adv. Mater. 2017, 29, 1701687.

S33. Zhu, Y. P.; Ma, T. Y.; Jaroniec, M.; Qiao, S. Z., Self-Templating Synthesis of Hollow Co_3O_4 Microtube Arrays for Highly Efficient Water Electrolysis. Angew. Chem. Int. Ed. 2017, 56, 1324-1328.

S34. Dong, C.; Kou, T.; Gao, H.; Peng, Z.; Zhang, Z., Eutectic-Derived Mesoporous Ni-Fe-O Nanowire Network Catalyzing Oxygen Evolution and Overall Water Splitting. Adv. Energy Mater. 2018, 8, 1701347.

S35. Li, H.; Wen, P.; Li, Q.; Dun, C.; Xing, J.; Lu, C.; Adhikari, S.; Jiang, L.; Carroll, D. L.; Geyer, S. M., Earth-Abundant Iron Diboride (FeB_2) Nanoparticles as Highly Active Bifunctional Electrocatalysts for Overall Water Splitting. Adv. Energy Mater.

2017, 7, 1700513.

S36. Menezes, P. W.; Panda, C.; Loos, S.; Bunschei-Bruns, F.; Walter, C.; Schwarze, M.; Deng, X.; Dau, H.; Driess, M., A structurally Versatile Nickel Phosphite Acting as a Robust Bifunctional Electrocatalyst for Overall Water Splitting. Energy Environ. Sci., 2018, 11, 1287-1298.

S37. Wu, L.-S.; Dai, H.-B.; Wen, X.-P.; Wang, P., Ni-Zn Alloy Nanosheets Arrayed on Nickel Foam as a Promising Catalyst for Electrooxidation of Hydrazine. ChemElectroChem 2017, 4 (8, 1944-1949.

S38. Zhou, L.; Shao, M.; Zhang, C.; Zhao, J.; He, S.; Rao, D.; Wei, M.; Evans, D. G.; Duan, X., Hierarchical CoNi-Sulfide Nanosheet Arrays Derived from Layered Double Hydroxides toward Efficient Hydrazine Electrooxidation. Adv. Mater. 2017, 29, 1604080.

S39. Liu, M.; Zhang, R.; Zhang, L.; Liu, D.; Hao, S.; Du, G.; Asiri, A. M.; Kong, R.; Sun, X., Energy-efficient Electrolytic Hydrogen Generation using a Cu_3P Nanoarray as a Bifunctional Catalyst for Hydrazine Oxidation and Water Reduction. *Inorg. Chem. Front.* 2017, 4, 420-423.

S40. Liu, G.; un, Z.; Zhang, X.; Wang, H.; Wang, G.; Wu, X.; Zhang, H.; Zhao, H., Vapor-phase Hydrothermal Transformation of a Nanosheet Array Structure $Ni(OH)_2$ into Ultrathin Ni_3S_2 Nanosheets on Nickel Foam for High-efficiency Overall Water Splitting. *J. Mater. Chem. A* 2018, 6, 19201-19209.

S41. Wang, G.; Chen, J.; Cai, P.; Jia, J.; Wen, Z., A self-supported Ni-Co Perselenide Nanorod Array as a High-activity Bifunctional Electrode for a Hydrogen-producing Hydrazine Fuel Cell. *J. Mater. Chem. A* 2018, 6, 17763-17770.

S42. Zhang, J.-Y.; Tian, X.; He, T.; Zaman, S.; Miao, M.; Yan, Y.; Qi, K.; Dong, Z.; Liu, H.; Xia, B. Y., *In situ* Formation of Ni_3Se_4 Nanorod Arrays as Versatile Electrocatalysts for Electrochemical Oxidation Reactions in Hybrid Water Electrolysis. *J. Mater. Chem. A* 2018, 6, 15653-15658.

S43. Sun, Q.; Wang, L.; Shen, Y.; Zhou, M.; Ma, Y.; Wang, Z.; Zhao, C., Bifunctional Copper-Doped Nickel Catalysts Enable Energy-Efficient Hydrogen Production via Hydrazine Oxidation and Hydrogen Evolution Reduction. *ACS Sustainable Chem. Eng.*

2018, 6, 12746−12754.

S44. Wang, J.; Khaniya, A.; Hu, L.; Beazley, M. J.; Kaden, W. E.; Feng, X., A Bifunctional Catalyst for Efficient Dehydrogenation and Electro-oxidation of Hydrazine. *J. Mater. Chem. A* 2018, 6, 18050-18056.

S45. Tang, C.; Zhang R.; Lu, W.; Wang, Z.; Liu, D.; Hao, S.; Gu, D.; Asiri, A. M.; Sun, X., Energy-Saving Electrolytic Hydrogen Generation: Ni_2P Nanoarray as a High-Performance Non-Noble-Metal Electrocatalyst. *Angew. Chem.* 2017, 129, 860–864.

S46. Wang, J.; Kong, R.; Asiri, A. M.; Sun, X., Replacing Oxygen Evolution with Hydrazine Oxidation at the Anode for Energy-Saving Electrolytic Hydrogen Production. ChemElectroChem 2017, 4, 481-484.

S47. Zhang, L.; Liu, D.; Hao, S.; Xie, L.; Qu, F.; Du, G.; Asiri, A. M.; Sun, X., Electrochemical Hydrazine Oxidation Catalyzed by Iron Phosphide Nanosheets Array toward Energy-Efficient Electrolytic Hydrogen Production from Water. ChemistrySelect 2017, 2 (12), 3401-3407.

S48. Ma, X.; Wang, J.; Liu, D.; Kong, R.; Hao, S.; Du, G.; Asiri, A. M.; Sun, X., Hydrazine-assisted Electrolytic Hydrogen Production: CoS_2 Nanoarray as a Superior Bifunctional Electrocatalyst. NewJ.Chem. 2017, 41, 4754-4757.

S49. Wang, J.; Ma, X.; Liu, T.; Liu, D.; Hao, S.; Du, G.; Kong, R.; Asiri, A. M.; Sun, X., NiS_2 Nanosheet Array: A high-active Bifunctional Electrocatalyst for Hydrazine Oxidation and Water Reduction toward Energy-efficient Hydrogen Production. Mater. Today Energy 2017, 3, 9-14.

S50. Feng, G.; Kuang, Y.; Li, Y.; Sun, X., Three-dimensional Porous Superaerophobic Nickel Nanoflower Electrodes for High-performance Hydrazine Oxidation. Nano Research 2015, 8, 3365-3371.

S51. Chen, S.; Duan, J.; Vasileff, A.; Qiao, S. Z. Size Fractionation of Two-Dimensional Sub-Nanometer Thin Manganese Dioxide Crystals towards Superior Urea Electrocatalytic Conversion, Angew. Chem. Int. Ed. 2016, 55, 3804–3808.

S52. Liu, T.; Liu, D.; Qu, F.; Wang, D.; Zhang, L.; Ge, R.; Hao, S.; Ma, Y.; Du, G.; Asiri, A. M.; Chen, L.; Sun, X., Enhanced Electrocatalysis for Energy-Efficient Hydrogen Production over CoP Catalyst with Nonelectroactive Zn as a Promoter. *Adv.*

Energy Mater. 2017, 7, 1700020.

S53. Xie, L.; Liu, Q.; Luo, Y.; Liu, Z.; Xu, Y.; Asiri, A. M.; Sun, X.; Xie, F., Bimetallic NiCoP Nanosheets Array for High-Performance Urea Electro-Oxidation and Less Energy-Intensive Electrolytic Hydrogen Production. ChemistrySelect 2017, 2, 10285-10289.

S54. Liu, Q.; Xie, L.; Qu, F.; Liu, Z.; Du, G.; Asiri, A. M.; Sun, X., A porous Ni_3N Nanosheet Array as a High-performance Non-noble-metal Catalyst for Urea-assisted Electrochemical Hydrogen Production. *Inorg. Chem. Front.* 2017, 4, 1120-1124.

S55. Liu, D.; Liu, T.; Zhang, L.; Qu, F.; Du, G.; Asiri, A. M.; Sun, X., High-performance Urea Electrolysis towards Less Energy-intensive Electrochemical Hydrogen Production using a Bifunctional Catalyst Electrode. J. Mater. Chem. A 2017, 5, 3208-3213.

S56. Hao, S.; Yang, L.; Liu, D.; Kong, R.; Du, G.; Asiri, A. M.; Yang, Y.; X. Sun, Integrating natural biomass electro-oxidation and hydrogen evolution: using a porous Fe-doped CoP nanosheet array as a bifunctional catalyst, Chem. Commun., 2017, 53, 5710-5713.

S57. You, B.; Jiang, N.; Liu, X.; Sun, Y., Simultaneous H_2 Generation and Biomass Upgrading in Water by an Efficient Noble-Metal-Free Bifunctional Electrocatalyst, *Angew. Chem. Int. Ed.* 2016, 55, 9913–9917.

S58. You, B.; Liu, X.; Liu, X.; Sun, Y., Efficient H_2 Evolution Coupled with Oxidative Refining of Alcohols via A Hierarchically Porous Nickel Bifunctional Electrocatalyst. ACS Catal. 2017, 7 (7), 4564-4570.